Syracuse University
SURFACE at Syracuse University

Physics - All Scholarship | Physics

Fall 11-13-2019

Loss of Vimentin Enhances Cell Motility through Small Confining Spaces

Alison E. Patteson
University of Pennsylvania, Syracuse University

Katarzyna Pogoda
University of Pennsylvania, Polish Academy of Sciences

Fitzroy J. Byfield
University of Pennsylvania

Kalpana Mandal
University of Pennsylvania

Zofia Ostrowska-Podhorodecka
University of Toronto

See next page for additional authors

Follow this and additional works at: https://surface.syr.edu/phy

 Part of the Physics Commons

Recommended Citation

Patteson AE, Pogoda K, Byfield FJ, Mandal K, Ostrowska-Podhorodecka Z, Charrier EE, Galie PA, Deptuła P, Bucki R, McCulloch CA, Janmey PA. Loss of Vimentin Enhances Cell Motility through Small Confining Spaces. Small. 2019 Dec;15(50):e1903180. doi: 10.1002/smll.201903180. Epub 2019 Nov 13. PMID: 31721440; PMCID: PMC6910987.

This Article is brought to you for free and open access by the Physics at SURFACE at Syracuse University. It has been accepted for inclusion in Physics - All Scholarship by an authorized administrator of SURFACE at Syracuse University. For more information, please contact surface@syr.edu.

Author(s)/Creator(s)
Alison E. Patteson, Katarzyna Pogoda, Fitzroy J. Byfield, Kalpana Mandal, Zofia Ostrowska-Podhorodecka, Elisabeth E. Charrier, Peter A. Galie, Piotr Deptuła, Robert Bucki, Christopher A. McCulloch, and Paul A. Janmey

This article is available at SURFACE at Syracuse University: https://surface.syr.edu/phy/548

Advertisement

Small / Volume 15, Issue 50 / 1903180

Full Paper | Full Access

Loss of Vimentin Enhances Cell Motility through Small Confining Spaces

Alison E. Patteson, Katarzyna Pogoda, Fitzroy J. Byfield, Kalpana Mandal, Zofia Ostrowska-Podhorodecka, Elisabeth E. Charrier, Peter A. Galie, Piotr Deptuła, Robert Bucki, Christopher A. McCulloch, Paul A. Janmey

First published: 13 November 2019
https://doi.org/10.1002/smll.201903180
Citations: 41

Go here for SU Links

Abstract

The migration of cells through constricting spaces or along fibrous tracks in tissues is important for many biological processes and depends on the mechanical properties of a cytoskeleton made up of three different filaments: F-actin, microtubules, and intermediate filaments. The signaling pathways and cytoskeletal structures that control cell motility on 2D are often very different from those that control motility in 3D. Previous studies have shown that intermediate filaments can promote actin-driven protrusions at the cell edge, but have little effect on overall motility of cells on flat surfaces. They are however important for cells to maintain resistance to repeated compressive stresses that are expected to occur in vivo. Using mouse embryonic fibroblasts derived from wild-type and vimentin-null mice, it is found that loss of vimentin increases motility in 3D microchannels even though on flat surfaces it has the opposite effect. Atomic force microscopy and traction force microscopy experiments reveal that vimentin enhances perinuclear cell stiffness while maintaining the same level of acto-myosin contractility in cells. A minimal model in which a perinuclear vimentin cage constricts along with the nucleus during motility through confining spaces, providing mechanical resistance

against large strains that could damage the structural integrity of cells, is proposed.

1 Introduction

Many important biological processes, such as embryogenesis,[1, 2] matrix remodeling,[3] and wound healing,[4, 5] depend on the ability of cells to move through the tight constricting spaces in tissues. This same ability can lead to cancer metastasis.[6, 7] During these biological events, cell migration is triggered through the epithelial–mesenchymal transition, in which nonmigratory epithelial cells lose cell–cell adhesions and transition to migratory polarized mesenchymal cells. A wide-spread marker of this transition is the intermediate filament protein vimentin.[8, 9] Vimentin expression is associated in vivo with wound healing[10] and cancer metastasis,[11] but its role in 3D motility remains unclear. Because cell motility is associated with changes in the mechanical properties of the cytoskeleton, determining vimentin mechanics at the single cell level is essential to understanding mechanisms that initiate migration and its contribution to proper tissue maintenance.

Intermediate filaments (IFs) are dispensable for cell motility and division of single cells in vitro,[12, 13] but are important for mechanical integrity on the multicellular and tissue scale.[13, 14] Cells on 2D flat surfaces covered by fluid primarily generate and resist traction stresses and deform to an extent governed by the shear modulus of the cytoskeleton, which is dominated by F-actin and modulated by microtubules.[12] In contrast, physical confinement in 3D causes changes to cell morphology and cytoskeletal structure, including cortical actin accumulation,[13] myosin II localization at the cell rear,[14] and reduction in cellular adhesion size.[13] Movement in 3D generally imposes compressive stresses on the cell and its nucleus[15, 16] as well as traction stresses at the leading and trailing edges.[17, 18] The role of vimentin in the resistance of cells to repeated compressive stresses[19] and the defective migration of cells in vimentin-null mice during wound healing[10] suggest that despite the modest effect of vimentin in cultured cells on flat surfaces,[20, 21] their effects in more physiologically relevant 3D settings might be more evident. This idea is supported by the mechanical properties of reconstituted cytoskeletal polymers. While IF are much softer compared to actin and microtubules at small strains, IF become significantly stiffer under large deformations and are capable of withstanding much larger strains without failure.[19, 22]

Here, we report the effects of vimentin on the 3D motility of cells. To determine the

contribution of vimentin, we used mouse embryonic fibroblasts (mEF) derived from wild-type (vim +/+) and vimentin-null (vim –/–) mice (**Figure** 1a). Unlike 2D studies, which show that loss of vimentin decreases motility,[20, 21] we show that loss of vimentin strongly increases motility in 3D environments. We measured cell stiffness using atomic force microscopy and found that vimentin stiffens the perinuclear region of the cell when bound to the substrate by collagen receptors. These results indicate that vimentin is an important regulator of 3D motility and resists mechanical stresses associated with pore migration.

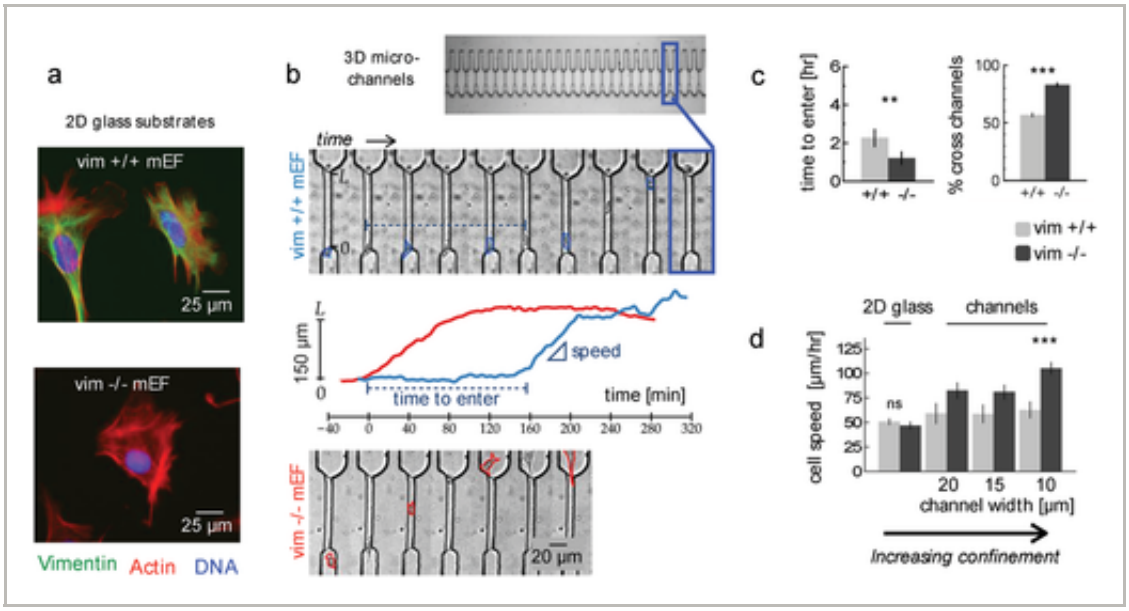

Figure 1

Open in figure viewer | PowerPoint

Loss of vimentin increases motility through constricting spaces. a) Immunofluorescence using antibodies against vimentin in wild-type (vim +/+) and vimentin-null (vim –/–) mouse embryonic fibroblasts (mEF). b) Arrays of microfluidic constrictions are embedded in PDMS chips and coated with collagen I. Bright-field time lapse images show vim +/+ and vim –/– mEF moving through microfluidic constrictions coated with collagen I (Movies S1 and S2, Supporting Information). The position of the cells along the channel was tracked manually over time, as shown by the sample blue curve for the wild-type cell and the red curve for the vimentin-null cell. The time to enter the channel and the speed in the channel were determined for each cell. c) Loss of vimentin decreases the time to enter the microchannels (16–40 cells per condition) and increases the percentage of cells that cross through (29–72 cells). Data for collagen-coated 10 μm channels from $N = 2$ experiments. d) Cell speed depends on the presence of vimentin and the degree of cell confinement. On flat glass slides, cell speeds are similar between wild-type and vimentin-null cells (45+ cells per condition, $N = 3+$ experiments). Cell speed increases with decreasing width of the microchannel. The speed of vimentin-null

cells is significantly larger compared to wild-type cells in the 10 μm channels (35–60 cells, $N = 2$).

2 Results

2.1 Loss of Vimentin Increases Cell Motility through Constricting Spaces

To model 3D cell motility, we designed microfluidic devices with micro-channels (Figure 1b). The channels can be coated with different extracellular ligand proteins and were designed to be large enough to allow the nucleus to pass through yet small enough to constrict the vimentin network ($W \times H \times L$: $10 \times 10 \times 150$ μm^3) (**Figure 2**). These channels mimic the dimensions of preexisting tracks in tissues[23] that have been observed as paths for neutrophil[24] and cancer cell[24, 25] migration. Inside the microchannel, the cell nuclei are more extended than on 2D glass substrates (Figure S1, Supporting Information), but the channel sizes are much greater than pores of 3 μm diameter where migration-induced nuclear damage has been observed. The channels were precoated with collagen I and seeded with either wild-type (vim +/+) or vimentin-null (vim –/–) mEF. No chemical gradients or pressure gradients were applied to the channels.

Both cell types spontaneously migrated into the microchannels (Figure 1b) with persistent motions lasting many hours (Movies S1 and S2, Supporting Information). This behavior, which has been called contact guidance, has been observed in many cell types.[26] To quantify the cell behavior, we tracked the position of cells over time and calculated the time for each cell to enter the channel and their speed inside the channel (Experimental Section). A fraction of the cells (<50%) became stuck or switched directions (Figure S2, Supporting Information) inside the channels (Movie S3, Supporting Information). Surprisingly, the loss of vimentin significantly increased migration through the channels. As shown in Figure 1c, cells lacking vimentin were able to enter the constrictions faster and had an increased probability of crossing through the channel.

To determine the effects of vimentin on confined cell motility, we measured cell speeds in microchannels with varying width (10, 15, and 20 μm) and compared to 2D glass slides (Figure 1d, Experimental Section). Cell speeds were measured inside the channels as a function of time; t, given by $|v(t)| = [r(t + \Delta t) - r(t)]/\Delta t$, where $\Delta t = 24$ min. Because cells sometime stop or stall in the channel, we choose the maximum instantaneous speed, $\max(|v(t)|)$, as a measure of persistent speed for each cell. Cells were categorized as inside

the microchannel when at least 80% of the spread area was within the channel. Here, cell speeds were statistically the same between the two cell types on 2D glass slides, although there might be a weak trend to lower speed for the vimentin –/– cells (Figure 1d).

Figure 2 Open in figure viewer | PowerPoint

Vimentin cytoskeleton in cells seeded in microchannels. Immunofluorescence images of vimentin in wild-type (vim +/+) and vimentin-null (vim –/–) mouse embryonic fibroblasts (mEF).

In the microchannels, the wild-type cell speeds depended only moderately on the channel width, increasing 1.2× with increasing confinement ($p = 0.058$). To check if this behavior was comparable to other cell lines, we used NIH 3T3 fibroblasts and found similar speeds and entrance times for the vim +/+ mEF as a function of channel width (Figure S3, Supporting Information). The vimentin-null cells displayed a sharp contrast. Their speeds rose strongly with confinement, increasing 2.25× ($p < 0.001$). Moderate confinement of cells (at length scales greater than the size of the nucleus) is known to increase the cell speed.[14, 26] This process corresponds with changes in the cytoskeletal organization, such as an enhancement of cortical actin and microtubule alignment with the substrate tracks. Here, loss of vimentin does not noticeably alter the shape of the cell in the channels, and the two cell lines have the same spread area inside the microchannels (Figure S4, Supporting Information). The large difference in speed in the microchannels (Figure 1) indicates that vimentin intermediate filaments also play a crucial role in 3D motility by reducing cell speeds.

2.2 Vimentin Hinders Migration in 3D Collagen Gel

To test the effects of vimentin on motility in fibrillar biopolymer matrices, we embedded the wild-type and vim –/– mEF in collagen I gels and tracked their motion over 17 h (Experimental Section). Bright-field images of the cells in the gel and sample trajectories are shown in **Figure** 3a. We quantified the cell motion by computing the cell speed as $|v(t)| = [r(t + \Delta t) - r(t)]/\Delta t$, where $\Delta t = 20$ min. We find that the speed of vimentin-null cells was greater than that of wild-type cells, indicating that loss of vimentin increased cell motility through 3D biopolymer gels.

Figure 3 Open in figure viewer | PowerPoint

Cell motility through 3D collagen gels. a) Bright-field images of vim +/+ and vim –/– mEFs cultured in 3D collagen gels (24 h, 2 mg mL^{-1}). Cell trajectories are gathered over 17 h. b) The speed of vimentin-null cells is greater than the speed of wild-type cells in the collagen networks (44–48 cells per condition, $N = 3$ experiments, $p < 0.01$). Error bars denote standard error. Denotation ***, $p < 0.001$; **, $p < 0.01$.

2.3 Vimentin Hinders Migration along Highly Curved Capillaries

In tissues, cells move within channel-like structures and along highly curved fibrous tracks such as nerves or small blood vessels. Since these two types of structures present opposite substrate curvature to the cell, we examined migration on glass capillaries with diameters ranging from 10 to 20 μm (**Figure** 4). Both cell lines tended to have a high aspect ratio and were elongated in the axial direction rather than the radial direction of the capillaries, possibly due to the high bending energy of F-actin (Figure 3a). Cells without vimentin moved more than three times faster on the capillaries (Figure 3b). Cell speeds were lower on the capillaries than in the microchannels (Figure 1d) but higher than the speeds in collagen gels (Figure 2b).

Figure 4 Open in figure viewer | PowerPoint

Loss of vimentin increases cell migration on highly curved capillaries. a) Bright-field time-lapse images of wild-type and vimentin-null mEF on collagen-coated capillaries, 15 μm in diameter. Scale bar, 30 μm. b) Vim –/– cells migrate faster than vim +/+ cells (17–27 cells per condition, $N = 2+$ independent experiments). Error bars denote standard error. Denotation ***, $p < 0.001$.

2.4 Vimentin Locally Increases Cell Stiffness

To provide insight to links between cell motility, vimentin expression, and the mechanical deformation of cells at the onset of entering a pore, we used atomic force microscopy (AFM) to measure the stiffness of normal and vimentin-null mEFs (**Figure** 5, Experimental Section). Intermediate filaments form densely packed networks that radiate to the cell periphery with decreasing density.[24] Previous studies with these cell lines applied minimal deformations on the cell cortex at the periphery of the cell and found no or little effect of vimentin on cell

stiffness. However, no difference may be expected at the cell periphery, since actin and microtubule expression levels are not affected in vim –/– mEF[27] and the vimentin network in a migrating cell is more abundant near the nucleus than at the cell periphery. Thus, we performed AFM tests focused on two regions of the cell: the endoplasmic region (between the nucleus and the cell periphery) and the region juxtaposed to the nucleus. We sampled in multiple positions to average over variations in the cytoskeleton (Figure 4a,b). In the endoplasmic region of the cell, the stiffness was ≈5 kPa and we did not detect differences by AFM between normal and vim –/– mEF (Figure S5, Supporting Information), consistent with prior investigations.[19] In the perinuclear region of the cell, however, we found a strong dependence on the presence of vimentin. The normal mEF stiffness was 2.5× times greater than that of vim –/– mEFs ($p < 0.001$). The data in Figure 4c demonstrate that vimentin can increase cell stiffness, particularly in the localized region around the nucleus.

Figure 5 Open in figure viewer | PowerPoint

Vimentin increases perinuclear cell stiffness coincident with decreased 3D migration. a) Immunofluorescence images of vim +/+ and vim –/– mEF, showing actin, microtubule, and vimentin staining on collagen-coated glass slides. b) An AFM tip was used to measure stiffness in the perinuclear region of the cell. Measurements were made at multiple positions per cell to account for variations in cytoskeletal structure (as marked). c) Wild-type mEFs were stiffer than vim –/– (30+ cells per condition, $N = 2+$ independent experiments). d) Cell speed decreases with cell stiffness for both the glass capillaries (circles) and microchannel (squares) experiments (dotted line to guide the eye). Wild-type mEF; blue symbols; vimentin-null mEF; red. Denotation ***, $p < 0.001$.

Our results demonstrate that vimentin contributes to cell stiffness, suggesting that vimentin may be involved in resisting mechanical stress during 3D cell migration. Combined with the motility assays, our results indicate that softer vimentin-lacking cells move faster than stiffer vimentin-containing cells in 3D environments (Figure 4d), a trend that is not observed on 2D surfaces (Figure 1d).

2.5 Cell Mechanical Tension Is Unaffected by Loss of Vimentin

To determine the effects of vimentin on the mechanical tension of the cell, we investigated

phosphorylated myosin activity and cellular traction stress in the vim +/+ and vim –/– mEF, as shown in **Figure** 6a,b, respectively. Figure 5a shows immunofluorescence images of phospho-myosin for cells on collagen-coated glass substrates. We observe large contractile stress fibers, which is typical for glass substrates, for both cell types. To quantify the level of myosin light chain activity, we performed Western blot experiments on the wild-type and vimentin-null mEF at 24 h time intervals (Experimental Section). We used β-actin as a measure of total cellular protein. Figure 5a shows the Western blot results for phospho-myosin light chain 2 (T18/S19) expression level at the 24 h time interval and densitometry quantification. The results show similar levels of phosphorylated myosin light chain in both wild-type and vimentin-null mEF, suggesting that the effect of vimentin loss on motility in channels and networks does not result from altered myosin activity. Next, we examined cell contractility by traction force microscopy (TFM) (Figure 5b). We found that the traction stress generated by vim –/– mEF was the same as that of vim +/+ cells on collagen-coated polyacrylamide surfaces. Overall, the results in Figure 4 indicate that the increase in cell motility due to the loss of vimentin (Figures 1 and 2) is not through changes in myosin activity or traction forces.

Figure 6 Open in figure viewer | PowerPoint

Myosin-II activity and traction stress in wild-type and vimentin-null cells. a) Immunofluorescence images of vim +/+ and vim –/– mEF, showing phosphorylated myosin, actin, and DNA staining after 24 h on collagen I-coated coverslips. Fold change quantifies the variation in pMLC levels from Western blots. Scale bar, 25 μm. Western blots of PP-myosin levels with control β-actin. b) Traction stress on collagen-coated 5 kPa polyacrylamide gels. (N = 2+ experiments; n = 20–28+ cells per condition. Error bars indicate standard error.)

2.6 Vimentin's Contribution to Perinuclear Stiffness Limits Cell Migration through Small Pores

Next, we examined confined cell migration through even smaller spaces associated with greater cellular strains by using Transwell membrane filters with pores sizes ranging from 3 to 8 μm in diameter. Cells were seeded on top of the membrane and allowed to migrate for 15 h before being fixed and counted (**Figure** 7a). We found that decreasing pore diameter generally suppressed pore migration for both cell types, but motility rates were significantly

higher in cells lacking vimentin compared to normal cells, for pore sizes both larger and smaller than the cell nucleus (Figure 6b). To check whether vimentin knockdown increases cell motility in other cell lines, we performed the Transwell experiments with wild-type and vimentin siRNA 3T3 cells (8 μm pores). Figure 6b shows that vimentin knockdown increased cell motility in 3T3 cells, indicating a predominant role of vimentin in hindering 3D cell motility.

Figure 7 Open in figure viewer | PowerPoint

Vimentin-mediated cell stiffness controls migration through small pores. a) Wild-type and vimentin-null mEF were seeded on top of Transwell membranes with pore diameters ranging from 3 to 8 μm. Cells were fixed and stained with crystal violet after 15 h. b) Loss of vimentin increases the percentage of mEF and NIH3T3 cells that migrate through 8 μm pores. c) The percentage of cells that cross the filter membrane, *k*, versus the compressional strain is captured by the proposed model.

Cells can migrate through physiologically confining spaces even when typical hallmarks of 2D migration, such as actin polymerization and myosin II-mediated contractility, are inhibited.[13] To determine whether the pore migration observed here depends on actomyosin contractility, we treated cells with the actin polymerization inhibitor cytochalasin D (Experimental Section) in the 5 μm pore filter assay and observed the change in % migration as a result of treatment (Figure S6, Supporting Information). For both vim +/+ and vim –/– mEFs, cell migration was reduced with cytochalasin D treatments, indicating that the regulation of contractile activity through actin polymerization and myosin filament assembly is important for the 3D motility observed here. Mounting evidence also shows a clear link between microtubules and 3D cell motility that differs from 2D motility.[28] To test the effect of microtubule polymerization on the 3D migration of vim +/+ and vim –/– mEFs, we treated cells with the microtubule inhibitor nocodazole and found a decrease in migration for both cell types.

To interpret the results, we propose a minimal model of constricted migration, assuming that the energy barrier to cross the pore is proportional to the cell stiffness *E* and the parameter $\varepsilon_0\varepsilon$, where ε is the compressional strain needed to cross the membrane and ε_0 is a prestrain based upon internal stresses that develop as cells adhere and spread on the

surface. The flux of cells then decreases by a factor exp($-\beta\varepsilon_0\varepsilon E$) for increasing cell stiffness E (a function of cell type) and strain ε (based on pore size).

Here, we estimate that the cell compressional strain varies from 0.47 to 0.80 based on the geometry of the pores (Figure 6c, Experimental Section). We fix the cell stiffness E to AFM values in the perinuclear region (Figure 3c). The curves in Figure 6b can be fit to $k_0\exp(-\beta\varepsilon_0\varepsilon E)$ for a single pair of constants, $\beta\varepsilon_0 = 0.24\ \text{kPa}^{-1}$ and $k_0 = 16\%$. The model captures the main features of the experimental data (Figure 6c), which further supports the idea that vimentin plays a predominant role in constricted cell migration through contributions to the cell stiffness.

3 Discussion

Intermediate filaments are involved in regulating the shape and structural integrity of the cell. Here, we found that vimentin plays an important role in modulating 3D motility. Our experiments with wild-type and vimentin-null mEFs show that vimentin reduces cell speed in small confining pores and along curved capillaries. This result is the opposite of the effect of vimentin on 2D substrates, where vimentin modestly enhances cell motility.[20, 21] Lack of vimentin or destabilization of the vimentin network on soft substrates[29] enhances lamellipodia formation, which on 2D substrates causes the cell to form lamellipodia in all directions without net cell displacements.[20] Whereas prior studies[20, 21] have observed a decrease in cell speed for cells lacking vimentin on 2D surfaces, it is not surprising that this effect is lessened in the immortalized cells used here (Figure 1d).

The strong effect of vimentin on 3D motility in the microchannels may be surprising given that intermediate filaments are much softer than F-actin or microtubules and thus easiest to deform to large strains. On the other hand, filamentous vimentin networks are less dynamic and more elastic compared to the more active actin and microtubule networks in the cytoskeleton. Thus, one might expect that the stable vimentin networks would resist squeezing through a small pore. This phenomenon is consistent with the mechanics of reconstituted vimentin networks that are especially soft at low strain, and significantly stiffen at large strains.[22]

Our experimental results motivate a physical mechanism based on the contribution of vimentin networks to cell stiffness. The good agreement between the migration data and our minimal model (Figure 6c) suggests that vimentin-mediated cell stiffness plays a

predominant role in 3D motility. This is most striking in Figure 1d, where the effects of vimentin grow with increasing cellular confinement. This trend suggests that strain-stiffening and resistance to breaking[22] may be the important mechanical features by which vimentin contributes to migration. While recent reports show that vimentin contributes to actin stress fiber formation through GEF-H1 and RhoA,[30] we found no difference in phospho-myosin expression and traction stresses between the wild-type and vimentin-null cells when on collagen-coated substrates. Vimentin intermediate filaments may also be modulating the assembly and function of the cytoskeleton in 3D settings. For instance, on 2D surfaces, vimentin contributes to organizing microtubule polarity,[31, 32] directing applied traction forces,[32] and regulating focal adhesion localization and dynamics.[24, 33-35]

Our results might seem counter-intuitive, considering that as epithelial cells undergo EMT and become more invasive, they upregulate vimentin. But vimentin expression is accompanied by a downregulation of cytokeratin, rather than upregulating intermediate filaments generally. Other IFs such as keratin have a larger effect on cell stiffness at the periphery, as deletion of keratin from epithelial cells leads to a large decrease in cortical stiffness measured by AFM[36] that is not seen with vimentin-containing mesenchymal cells. Recent studies have shown that disruption of keratin networks in pancreatic cancer cells enhances cell deformability and migration in microchannels,[37] which correlates with increased metastatic potential. One possible explanation for the upregulation of vimentin is its greater localization around the nucleus compared to other cytoskeletal filaments, which may be required to cushion the nucleus or the cortical actin network during extreme strains associated with confined migration.

During in vivo cell migration, the cell and the nucleus undergo large strains in order to squeeze through small pores or conform to fibrous tracks.[15, 16, 38] Migration through tight spaces below 3 μm can lead to nuclear damage, such as nuclear envelope rupture, accumulated double-stranded DNA breaks, and changes in genome variation.[15, 16, 38] Here, the nuclear volumes of the mEF correspond to a nuclear diameter of ≈8 μm or less, assuming a spherical shape. Therefore, the deformation of the nucleus itself should be minimal through an 8 μm pore but much larger in the 3 μm pores. The hindrance to motion of the wild-type cells in the microchannels (Figure 1), which are 10–20 μm in width, suggest that some structure larger than the nucleus needs to be deformed in order for the cell to transit, consistent with the idea that the composite of the nucleus and its perinuclear vimentin cage acts as a coherent physical structure.

It is now well accepted that the nuclear lamina plays an important role in controlling the rate of 3D cell migration and promotes cell survival by protecting the nucleus against migration-induced stresses.[34] Similarly, high resistances to compressive stresses could be the main advantage of vimentin expression during 3D migration. Intermediate filaments are connected with nuclear lamina through nesprins and plectins.[39] Vimentin's role in resisting stress thereby likely contributes to mechanical force transmission between the cytoskeleton and the nuclear interior and may be involved in anchoring and immobilizing the nucleus. Our current work[40] reveals that the loss of vimentin increases nuclear damage, such as nuclear membrane rupture, during pore migration. Therefore, low susceptibility to compressive stresses could be the main advantage of vimentin expression during 3D migration. The mechanical properties of the nuclear lamina combined with the presence of the juxtanuclear vimentin cage may represent an example of redundancy, which is often observed for biological phenomena with functional importance. Overall, our findings indicate that vimentin's perinuclear stiffness controls 3D motility and provides new insight into how cells might alter their cytoskeleton to maximize invasion in vivo without compromising cell integrity.

4 Conclusion

In summary, we find that loss of vimentin intermediate filaments enhances cell motility in 3D environments even though on 2D surfaces it has the opposite effect. Localized atomic force microscopy measurements in the perinuclear region of the cell show that vimentin enhances cell stiffness in the region around the nucleus but not in the cell cortex. We therefore propose that the nonlinear strain stiffening properties of vimentin impede migration through small pores even when their size exceeds the diameter of the nucleus. Overall, our findings indicate that vimentin expression may act not to increase actin-dependent cell speed during 3D cell migration in vivo but to protect the cell and its nucleus from structural damage from the corresponding extreme strains. These results indicate that the mechanical properties of intermediate filaments should be taken into consideration when developing and evaluating 3D cell migration models.

5 Experimental Section

Cell Culture: Wild-type mEF and vimentin-null mEF were kindly provided by J. Ericsson (Abo Akademi University, Turku, Finland) and maintained in DMEM with 25×10^{-3} M HEPES and sodium pyruvate (Life Technologies, Grand Island, NY) supplemented by 10% fetal bovine

serum, 1% penicillin streptomycin (Gibco), and nonessential amino acids (Life Technologies). For NIH-3T3 fibroblasts (American Type Culture Collection, Manassas, VA), cells were maintained in DMEM (Gibco) with 10% fetal bovine serum (ATCC) and 1% penicillin streptomycin, and 25×10^{-3} M HEPES was added to media for microchannel experiments. All cell cultures were maintained at 37 °C and 5% CO_2. NIH 3T3 fibroblasts were transfected with VIM-specific siRNA (ON TARGET plus siRNA- Dharmacon) according to the manufacturer's instructions.

Immunofluorescence: Cells were fixed for immunofluorescence using 4% paraformaldehyde for 30 min at 37 °C, permeabilized with 0.05% Triton X-100 solution in PBS (15 min, room temperature RT), and saturated with 1% serum albumin bovine (30 min, RT). For vimentin visualization, cells were incubated with primary anti-vimentin monoclonal rabbit antibody (1:200, RT, Abcam ab92547) or primary anti-vimentin polyclonal chicken antibody (1:200, RT, Novus NB300-223); secondary antibodies were anti-Rabbit Alexa Fluor 488 (1:1000, RT, Invitrogen A-11008) or anti-chicken Alexa Fluor 488 (1:1000, RT, Invitrogen A-11039). For visualizing microtubules, primary anti-tubulin monoclonal rat antibody (1:200, Serotec MCA77G) and secondary anti-rat AlexaFluor647 (Invitrogen A-21247) were used. For immunostaining cells in microchannels and on capillaries, primary antibodies were diluted to 1:1000 and kept overnight at 4 °C. Cells were washed and stained with Rhodamine phalloidin 565 (Life Tech. r415) or Texas Red phalloidin and Hoechst 33342 (Molecular probes H-1399) or DAPI (Molecular probes) for 1 h according to manufacturer's instructions. Cells were imaged with a Leica DMIRE2 inverted microscope with either a 40× (0.55 NA) air objective lens or 63× (0.70 NA) air objective lens.

Microfluidic Device Fabrication and Operation—Fabrication: The microfluidic devices were built using standard soft lithography techniques and designed to prevent pressure gradients across the channels as described in the study of Irimia et al.[41] The positive silicon master was generated by spinning KMPR 2010 onto silicon wafers (Wafer World Inc., West Palm Beach, FL) to create a 10 μm thick layer. The photoresist was soft baked for 5 min at 95 °C and exposed to UV light through a chrome mask (CAD/Art Services, Inc.) with a mask aligner (ABM-USE, Inc., ABM3000HR). Unexposed KMPR2010 was developed with SU-8 developer and rinsed with isopropanol. This process was repeated two times in order to stack the three layers of the device that were aligned with a mask aligner (Figure S1, Supporting Information). The positive wafer obtained was silanized (Sigma 448931) in a vacuum chamber overnight. A PDMS (Sylgard 184) solution at a 1:10 ratio (curing:elastomer) was mixed and degassed. This solution was then poured over the silanized positive silicon wafer

and baked 90 min at 80 °C to generate a negative mold. The negative mold was silanized overnight in a vacuum chamber. This protocol was repeated to obtain the silanized positive mold that was used to build the microfluidic device. Finally, a PDMS mixture was degassed, poured over the PDMS positive molds, baked for 90 min at 80 °C, and removed from the mold. The device was punched with 0.5 mm access holes for tubing inserts. Channels were sealed with a glass microscope slide using an oxygen plasma chamber (Femto-Diener Electronic).

Microfluidic Device Fabrication and Operation—Operation: To sterilize and clean the device, it was flushed with a solution of 70% (vol/vol) ethanol in deionized water (diH_2O), followed by rinsing with sterile diH_2O. Next, the device was submerged in sterile diH_2O and degassed to remove bubbles. Channels were then rinsed with phosphate buffered saline (PBS) and coated with surface ligands by pumping in a 50 μg mL^{-1} solution of collagen I (BD Biosciences, Franklin Lakes, NJ) in PBS and incubating for 1 h at 37 °C. Finally, channels were then washed 3× with PBS, filled with cell culture media, and incubated at 37 °C for at least 30 min before seeding cells.

Microfluidic Device Fabrication and Operation—Cell Culturing and Seeding: Cells were trypsinized using 0.5% trypsin (GIBCO) at 37 °C, centrifuged to remove trypsin, and resuspended in cell media at densities of 1×10^6 million cells mL^{-1}. Using a hand-held syringe (Hamilton Company, 81320) and tubing (Hamilton Company, 90622), cells were gently pumped into the device inlet. Cells were preferentially placed near the opening of the channel constrictions by manually tilting the device for 2 to 4 min and allowing gravity to pull cells in suspension toward the constrictions. Fluid reservoirs (barrel-less syringes (BD, Ref. 309657) containing cell media) were connected to the channel outlets with tubing and arranged to ensure no pressure driven flow through the channels. The device was kept in a Tokai-Hit Imaging Chamber (Tokai Hit, Shizuoka-ken, Japan) and maintained at 37 °C and 5% CO_2. Cells were allowed to adhere to channel surfaces for ≈20–40 min before time-lapse imaging began. Time-lapse imaging was performed with a Leica DMIRE2 inverted microscope in bright field with a 10× (0.3 NA) air lens. Images were taken every 4 min for 12–21 h using an ASI *x*/*y*/*z* stage (MS – 2000, Applied Scientific Instrumentation) to capture multiple positions in the device.

Capillary Fabrication and Operation—Fabrication: Capillaries having diameters ranging from 10 to 20 μm were pulled from larger borosilicate glass capillaries with a diameter of 1.6 mm (Richland Glass, Richland, NJ) using a Narishige PB-7 pipette puller. Cell culture chambers

(length 60 mm, width 240 mm, height 12 mm) were printed using either ABS or PLA plastic (Biomedical library, University of Pennsylvania). To allow for visualization of the cells, windows were designed into the upper and lower sections of the chambers. Capillaries were affixed to the inner surface of the chambers using UV-curable glue (NOA 68, Norland Products).

Capillary Fabrication and Operation—Operation: Capillaries were cleaned by rinsing once with ethanol, then rinsing with deionized H_2O, and then air dried. Chambers containing capillaries were then placed in a plasma cleaner (Harrick, PDC-32G) and exposed to air plasma for 5 min. Overnight incubations with 0.1 mg mL^{-1} collagen were then made while shaking on an orbital shaker. Capillaries were then rinsed 3× with PBS, sterilized under UV for 1 h, and then incubated with culture media for at least 10 min before cell seeding.

Capillary Fabrication and Operation—Cell Culturing and Seeding: Cells were trypsinized using 0.5% trypsin (GIBCO) at 37 °C then centrifuged to remove trypsin. Resuspended cells at a density of 2.5×10^5 cells mL^{-1} were added to the capillaries and allowed to attach for 60 min at 37 °C. Cell culture chambers were then transferred to a Tokai-Hit Imaging Chamber mounted on an ASI *x*/*y*/*z* stage and maintained at 37 °C and 5% CO_2. Time-lapse images were taken at multiple positions every 10 min for 18–21 h using a 40× objective.

Cell Area and Motility Measurements—Cell Area: The projected cell area changed over time as the cell entered and moved through the channel (Figure S4, Supporting Information). Thus, cell area at three designated points was measured: (i) 1 h before cells entered the channel, (ii) at the middle of the channel length, and (iii) 1 h after cell exited the channel. Cell area was determined by manually tracing the periphery of single cells (N = 25–35 cell per condition) using ImageJ software (ImageJ Software, NIH, Bethesda, MD).

Cell Area and Motility Measurements—Cell Speed in Microchannels, Glass Slides, and Capillaries: Cell trajectories were determined by tracking the center of mass of cells at either 4 or 10 min increments using ImageJ Software (NIH) and the Manual Tracking plugin (**https://imagej.nih.gov/ij/**). Here, cell speed was determined over time t as $|v(t)| = [r(t + \Delta t) - r(t)]$, where Δt was ≈24 min. To compare the directed cell motion in the 3D environments (microchannels and capillaries) with the more random motion in 2D (glass slides), the maximum value of $|v(t)|$ was chosen as the measure of cell speed for each cell in each experimental condition. Cells that divided or moved out of the frame of view were excluded.

3D Collagen Gel Preparation and Imaging—Gel Preparation: Collagen gels (2 mg mL^{-1}) were

prepared with final concentrations of 300 000 cells mL^{-1} by mixing together the following reagents in the order listed: pelleted and counted cells in media (10% v/v), 5× DMEM (20% v/v), FBS (10% v/v), 0.1 M NaOH (10% v/v), and 4 mg mL^{-1} collagen type 1 (Corning, Ref. 354236, 50%v/v). Reagents were kept cold on ice while mixing. 1 mL of mixture was added to 20 mm dishes and maintained at 37 °C and 5% CO_2. Cells were imaged in bright field, 24 h after seeding in gel (Figure 1).

3D Collagen Gel Preparation and Imaging—Imaging Nucleus for Tracking in Gels: To track cells in the 3D gels over time, the nuclei of vim +/+ and vim –/– mEF were fluorescently labeled with NLS-GFP. For these experiments, cells were transiently transfected with pEGF-C1-NLS kindly provided by Robert Goldman (Northwestern University). 48 h after transfection, cells were cultured in the collagen gel. 24 h later, cell nuclei were imaged at 10 min increments for 17 h by using fluorescence microscopy and a 10× (0.3 NA) air lens. Cells observed to move out of the field of view, divide, or die were excluded. Experiments were conducted three times for a total of 44–48 cells per condition.

Cell Stiffness Measurements: Cell perinuclear stiffness measurements were performed using atomic force microscopy (NanoWizard 4, JPK) equipped with a liquid cell and temperature control setup. Silicon nitride cantilevers (ORC8, Bruker) with nominal 0.1 N m^{-1} spring constant and tip half-opening angle of 36° ± 2° were used for cell nanoindentation. Quantitative characterization of nanomechanical properties of the cells was realized by recording of multiple force versus distance curves in the perinuclear region (Figure 3b) with the constant force of 3 nN and indentation rate equal 0.4 Hz. Modified Hertz model was fitted to the data, and Young's modulus of each point was calculated as described previously.[42]

Cell Traction Force Measurement—Materials and Methods: To measure cell traction forces exerted by the cell, 5 kPa polyacrylamide (PAA) hydrogel substrates were prepared as described previously.[43, 44] Briefly, 8% acrylamide and 0.1% bis-acrylamide (Bio-Rad), 0.375% 3 ammonium persulfate (Thermo Fisher Scientific), and 0.125% tretramethylethylenediamine (Millipore sigma) are mixed in water to prepare the gels. In addition, 1% of 200 nm fluorescently labeled green beads (2% solid, Thermo Fisher Scientific) was added before gelation and the solution was left for 30 min to 1 h for polymerization at RT. Sulfo-SANPAH was used for gel surface activation to facilitate protein conjugation for 3–5 min under UV illumination. Gels were laminated with rat tail collagen I at a concentration of 100 µg mL^{-1}. After 24 h of seeding, phase images and fluorescence images of the beads were acquired

before and after removal of the cells to relieve traction stress. For the TFM analysis, a custom-built Matlab code was used. The details of the calculation can be found in refs. 43, 45. Briefly, the displacement field is calculated from stressed and relaxed images of the beads. A 32 × 32 pixel ROI was used for the image correlation calculation. By constrained Fourier transform traction microscopy (FTTM) the cell traction field was obtained from the displacement field.

Transwell Migration Assays: Cells were seeded at subconfluent concentrations (10–20 thousand cells cm^{-2}) on polycarbonate Transwell membranes with pore diameters of 3 μm (Corning, CLS3414), 5 μm (Corning, CLS3421), and 8 μm (Corning, CLS3428). Membranes were precoated with collagen I (50 μg mL^{-1}). After seeding cells, the filters were maintained at 37 °C and 5% CO_2 for 15 h. Cells were gently removed from either the top or bottom of the membrane with a cotton swab and immediately fixed with paraformaldehyde. To determine the number of cells per unit area, cells were stained with crystal violet and imaged at multiple locations across the membrane with a 10× objective. Cells were manually counted in 800 × 800 $μm^2$ fields of view (12–30 locations per condition). The percentage of cells that cross the membrane (Figure 4) was then determined by taking the ratio of the number of cells on the bottom of the membrane and the sum of cells on the filter top and bottom.

Transwell Migration Assays—Estimate of Compressional Cell Strain: To estimate the cell strain through the Transwell filters, it was assumed that the cells maintain a constant volume of 1.76 pL (equivalent to a sphere of diameter 15 μm). This volume is less than the value determined by multiplying the average cell spread area by the channel height, which yields an overestimate of 2.1 ± 0.2 pL for vim +/+ mEF and 2.4 ± 0.2 pL for vim –/– mEF. Compressional cell strain is then estimated as the magnitude of $(L_1 - L)/L$, where L is the cell size in the unstressed spherical state (15 μm) and L_1 is the narrowest dimension of the cell while crossing the pore, the diameter of the pore (cf. Figure 6).

Transwell Migration Assays—Inhibitor Treatments: Cells were placed in 5 μm pore Transwell assays for 2 h. Then, cells were treated with either blebbistatin (50×10^{-6} M), cytochalasin D (1 μg mL^{-1}), or nocodazole (1 μg mL^{-1}). Cells were fixed and stained at 15 h. Controls were performed alongside each treatment. Experiments were conducted a minimum of two times per condition.

Western Blots: 3.9×10^5 mEF VIM+/+ and mEF VIM –/– cells were plated for 3 and 24 h on 100 mm dishes coated with 50 mg mL^{-1} collagen. Total cell lysates were prepared by harvesting

cells in SDS lysis buffer (0.5% SDS, 50×10^{-3} M Tris-HCl pH 8.0, 10×10^{-3} M EDTA pH 8.0, 1×10^{-3} M PMSF, 1×10^{-3} M Na_3VO_4, and 1:50 protease inhibitor cocktail (Sigma Aldrich)). Protein concentration was determined using the Pierce BCA Protein Assay Kit (Thermo Scientific). Protein extracts were mixed with 4× SDS sample buffer (Tris pH 6.8, 1.7% SDS, glycerol and 1×10^{-3} M DTT), and the cell lysates were resolved on 15% SDS-polyacrylamide gels of 1.5 mm thickness. Proteins were then transferred onto nitrocellulose membrane (GE Healthcare Amersham Protran NC Nitrocellulose Membranes) and subsequently blocked with 5% skim milk in TBST (20×10^{-3} M Tris, 150×10^{-3} M NaCl, and 0.05% Tween 20; pH 7.4) for 1 h at room temperature. The membranes were incubated overnight at 4 °C with primary antibodies, then at room temperature for 1 h with the secondary antibodies. The primary antibodies used in this study were as follows: anti-P-Myosin Light Chain 2 (T18/S19) (rabbit monoclonal; 1:1000; Cell Signaling), anti-P-Myosin Light Chain 2 (S19) (Mouse monoclonal; 1:1000; Cell Signaling), anti-Myosin Light Chain 2 (Rabbit monoclonal; 1:1000; Cell Signaling), and anti-β- actin (Mouse monoclonal; 1:5000; Cell Signaling). Goat anti-mouse IRDye 680 RD (1:1000; Odyssey) and Goat anti-Rabbit IRDye 800 CW (1:5000, Li-Core) were used as the secondary antibodies. Protein bands were visualized using Li-Core Biosciences software. Antibody intensities were normalized by anti-β-actin intensities for each condition. Fold change is determined with respect to the wild-type mEFs.

Statistical Analysis: Data are presented as mean values ± standard errors (SE). Each experiment was performed a minimum of two times unless otherwise stated. The unpaired Student's *t*-test with two tails at the 95% confidence interval was used to determine statistical significance. Denotations: *, $p <= 0.05$; **, $p < 0.01$; ***, $p < 0.001$; ns, $p > 0.05$.

Acknowledgements

This work was supported by the National Institutes of Health-National Institute of General Medical Sciences (P01 GM096971), the U.S. National Science Foundation (CMMI-154857 and DMR-1720530), and the National Science Center, Poland under Grant No. UMO-2015/17/B/NZ6/03473 (to RB) and UMO-2016/26/D/ST4/00997 (to KP). The authors thank Dennis Discher and Manu Tewari for help amplifying the pEGF-C1-NLS plasmid. The authors also thank Eric Johnston and Nathan Bade for help developing the microfluidic device and Mateusz Cieśluk for his technical assistance during AFM experiments. The authors kindly thank Arvind Gopinath, Ravi Radhakrishnan, and Jennifer Schwarz for insight and feedback on the motility model. A.E.P. designed, performed, and analyzed motility experiments using microfluidics devices and Transwell membrane assays. F.B. designed and performed

capillary experiments and analysis. K.P., R.B., and P.D. designed and performed AFM measurements and analysis. K.M. performed and analyzed TFM measurements. E.C. and P.G. developed microfluidic device. Z.O. and C.M. performed Western blot detection of phospho-myosin. A.E.P., F.B., K.P., E.C., P.G., and P.A.J. contributed to project design and wrote the manuscript.

Conflict of Interest

The authors declare no conflict of interest.

Supporting Information

Filename	Description
smll201903180-sup-0001-SuppMat.pdf807.6 KB	Supporting Information
smll201903180-sup-0002-VideoS1.avi657.7 KB	Supplementary Video 1
smll201903180-sup-0003-VideoS2.avi570.1 KB	Supplementary Video 2
smll201903180-sup-0004-VideoS3.avi719.1 KB	Supplementary Video 3

Please note: The publisher is not responsible for the content or functionality of any supporting information supplied by the authors. Any queries (other than missing content) should be directed to the corresponding author for the article.

References

1 J. Yang, R. A. Weinberg, *Dev. Cell* 2008, **14**, 818.

2 J. P. Thiery, H. Acloque, R. Y. J. Huang, M. A. Nieto, *Cell* 2009, **139**, 871.

3 F. Cheng, J. E. Eriksson, *Cold Spring Harbor Perspect. Biol.* 2017, **9**, a022046.

4 S. Lamouille, J. Xu, R. Derynck, *Nat. Rev. Mol. Cell Biol.* 2014, **15**, 178.

5 M. T. Abreu-Blanco, J. J. Watts, J. M. Verboon, S. M. Parkhurst, *Cell. Mol. Life Sci.* 2012, **69**, 2469.

6 P. Friedl, D. Gilmour, *Nat. Rev. Mol. Cell Biol.* 2009, **10**, 445.

7 C. D. Paul, P. Mistriotis, K. Konstantopoulos, *Nat. Rev. Cancer* 2017, **17**, 131.

8 M. G. Mendez, S.-I. Kojima, R. D. Goldman, *FASEB J.* 2010, **24**, 1838.

9 E. D. Hay, *Dev. Dyn.* 2005, **233**, 706.

10 B. Eckes, E. Colucci-Guyon, H. Smola, S. Nodder, C. Babinet, T. Krieg, P. Martin, *J. Cell Sci.* 2000, **113**, 2455.

11 A. Satelli, S. Li, *Cell. Mol. Life Sci.* 2011, **68**, 3033.

12 M. L. Gardel, I. C. Schneider, Y. Aratyn-Schaus, C. M. Waterman, *Annu. Rev. Cell Dev. Biol.* 2010, **26**, 315.

13 E. M. Balzer, Z. Tong, C. D. Paul, W. C. Hung, K. M. Stroka, A. E. Boggs, S. S. Martin, K. Konstantopoulos, *FASEB J.* 2012, **26**, 4045.

14 Y.-J. Liu, M. Le Berre, F. Lautenschlaeger, P. Maiuri, A. Callan-Jones, M. Heuzé, T. Takaki, R. Voituriez, M. Piel, *Cell* 2015, **160**, 659.

15 M. Raab, M. Gentili, H. de Belly, H. R. Thiam, P. Vargas, A. J. Jimenez, F. Lautenshlaeger, R. Voituriez, A. M. Lennon-Dumenil, N. Manel, M. Piel, *Science* 2016, **352**, 359.

16 C. Denais, R. M. Gilbert, P. Isermann, A. L. McGregor, M. te Lindert, B. Weigelin, P. M. Davidson, P. Friedl, K. Wolf, J. Lammerding, *Science* 2016, **352**, 353.

17 P. S. Raman, C. D. Paul, K. M. Stroka, K. Konstantopoulos, *Lab Chip* 2013, **13**, 4599.

18 M. S. Hall, F. Alisafaei, E. Ban, X. Feng, C.-Y. Hui, V. B. Shenoy, M. Wu, *Proc. Natl. Acad. Sci. USA* 2016, **113**, 14043.

19 M. G. Mendez, D. Restle, P. A. Janmey, *Biophys. J.* 2014, **107**, 314.

20 B. T. Helfand, M. G. Mendez, S. N. P. Murthy, D. K. Shumaker, B. Grin, S. Mahammad, U. Aebi, T. Wedig, Y. I. Wu, K. M. Hahn, M. Inagaki, H. Herrmann, R. D. Goldman, *Mol. Biol. Cell* 2011, **22**,

1274.

21 B. Eckes, D. Dogic, E. Colucci-Guyon, N. Wang, A. Maniotis, D. Ingber, A. Merckling, F. Langa, M. Aumailley, A. Delouvee, V. Koteliansky, C. Babinet, T. Krieg, *J. Cell Sci.* 1998, **111**, 1897.

22 P. A. Janmey, U. Euteneuer, P. Traub, M. Schliwa, *J. Cell Biol.* 1991, **113**, 155.

23 K. Wolf, S. Alexander, V. Schacht, L. M. Coussens, U. H. von Andrian, J. van Rheenen, E. Deryugina, P. Friedl, *Semin. Cell Dev. Biol.* 2009, **20**, 931.

24 P. Friedl, E.-B. Bröker, *Dev. Immunol.* 2000, **7**, 249.

25 B. Weigelin, G.-J. Bakker, P. Friedl, *IntraVital* 2012, **1**, 32.

26 D. Irimia, M. Toner, *Integr. Biol.* 2009, **1**, 506.

27 M. Guo, A. J. Ehrlicher, S. Mahammad, H. Fabich, M. H. Jensen, J. R. Moore, J. J. Fredberg, R. D. Goldman, D. A. Weitz, *Biophys. J.* 2013, **105**, 1562.

28 B. P. Bouchet, A. Akhmanova, *J. Cell Sci.* 2017, **130**, 39.

29 M. E. Murray, M. G. Mendez, P. A. Janmey, *Mol. Biol. Cell* 2014, **25**, 87.

30 Y. Jiu, J. Peränen, N. Schaible, F. Cheng, J. E. Eriksson, R. Krishnan, P. Lappalainen, *J. Cell Sci.* 2017, **130**, 892.

31 N. Costigliola, L. Ding, C. J. Burckhardt, S. J. Han, E. Gutierrez, A. Mota, A. Groisman, T. J. Mitchison, G. Danuser, *Proc. Natl. Acad. Sci. USA* 2017, **114**, 5195.

32 C. De Pascalis, C. Pérez-González, S. Seetharaman, B. Boëda, B. Vianay, M. Burute, C. Leduc, N. Borghi, X. Trepat, S. Etienne-Manneville, *J. Cell Biol.* 2018, **217**, 3031.

33 P. M. Davidson, C. Denais, M. C. Bakshi, J. Lammerding, *Cell Mol. Bioeng.* 2014, **7**, 293.

34 T. Harada, J. Swift, J. Irianto, J.-W. Shin, K. R. Spinler, A. Athirasala, R. Diegmiller, P. C. D. P. Dingal, I. L. Ivanovska, D. E. Discher, *J. Cell Biol.* 2014, **204**, 669.

35 K. Wolf, M. te Lindert, M. Krause, S. Alexander, J. te Riet, A. L. Willis, R. M. Hoffman, C. G. Figdor, S. J. Weiss, P. Friedl, *J. Cell Biol.* 2013, **201**, 1069.

36 K. Seltmann, A. W. Fritsch, J. A. Käs, T. M. Magin, *Proc. Natl. Acad. Sci. USA* 2013, **110**, 18507.

37 C. G. Rolli, T. Seufferlein, R. Kemkemer, J. P. Spatz, *PLoS One* 2010, **5**, e8726.

38 J. Irianto, Y. Xia, C. R. Pfeifer, A. Athirasala, J. Ji, C. Alvey, M. Tewari, R. R. Bennett, S. M. Harding, A. J. Liu, R. A. Greenberg, D. E. Discher, *Curr. Biol.* 2017, **27**, 210.

39 K. Wilhelmsen, S. H. M. Litjens, I. Kuikman, N. Tshimbalanga, H. Janssen, I. van den Bout, K. Raymond, A. Sonnenberg, *J. Cell Biol.* 2005, **171**, 799.

40 A. E. Patteson, A. Vahabikashi, K. Pogoda, S. A. Adam, K. Mandal, M. Kittisopikul, S. Sivagurunathan, A. Goldman, R. D. Goldman, P. A. Janmey, *J. Cell Biol.* 2019, jcb.201902046.

41 D. Irimia, G. Charras, N. Agrawal, T. Mitchison, M. Toner, *Lab Chip* 2007, **7**, 1783.

42 K. Pogoda, J. Jaczewska, J. Wiltowska-Zuber, O. Klymenko, K. Zuber, M. Fornal, M. Lekka, *Eur. Biophys. J.* 2012, **41**, 79.

43 K. Mandal, I. Wang, E. Vitiello, L. A. C. Orellana, M. Balland, *Nat. Commun.* 2014, **5**, 5749.

44 K. Mandal, D. R.-B. Aroush, Z. T. Graber, B. Wu, C. Y. Park, J. J. Fredberg, W. Guo, T. Baumgart, P. A. Janmey, *ACS Nano* 2018, **13**, 203.

45 J. P. Butler, I. M. Tolić-Nørrelykke, B. Fabry, J. J. Fredberg, *Am. J. Physiol.* 2002, **282**, C595.

Citing Literature

Download PDF

ABOUT WILEY ONLINE LIBRARY

Privacy Policy
Terms of Use
About Cookies
Manage Cookies
Accessibility
Wiley Research DE&I Statement and Publishing Policies
Developing World Access

HELP & SUPPORT

Contact Us
Training and Support
DMCA & Reporting Piracy

OPPORTUNITIES

Subscription Agents
Advertisers & Corporate Partners

CONNECT WITH WILEY

The Wiley Network
Wiley Press Room

WILEY

Copyright © 1999-2023 John Wiley & Sons, Inc. All rights reserved